Biophysical Journal
Article

Biophysical Society

Effects of Nanopore Charge Decorations on the Translocation Dynamics of DNA

Ining Jou[1] and Murugappan Muthukumar[1,*]
[1]Department of Polymer Science and Engineering, Conte Research Center, University of Massachusetts, Amherst, Massachusetts

ABSTRACT We have investigated the dynamics of single-stranded DNA as it translocates through charge-mutated protein nanopores. Translocation of DNA is a crucial step in nanopore-based sequencing platforms, where control over translocation speed remains one of the main challenges. Taking advantage of the interactions between negatively charged DNA and positively charged amino acid residues, the translocation speed of DNA can be manipulated by deliberate charge decorations inside the nanopore. We employed coarse-grained Langevin dynamics simulations to monitor the step-by-step movement of DNA through different mutations of α-hemolysin protein nanopores. We found that although the average translocation time per nucleotide is longer, in agreement with experiments, the DNA nucleotides do not translocate with a uniform speed. Furthermore, the location and spacing of the charge decorations can alter the translocation dynamics significantly, trapping DNA in some cases. Our findings can give insights when designing charge patterns in nanopores.

INTRODUCTION

Nanopore-based technology is emerging as a versatile tool in single-molecule sensing and characterization (1–4). One of the most remarkable applications offers label-free (5), amplification-free (6,7), and real-time (8) sequencing of DNA. The main idea behind this application is that as a single-stranded DNA (ssDNA) molecule is electrophoretically driven through a nanopore, the signal of the ionic current trace is modified by the passage of different nucleotides (9). Recent advances in both biological and solid-state nanopores are bringing us closer to a cheaper, faster, and highly accurate nanopore platform for DNA sequencing (7,10,11).

It has been shown that biological nanopores are able to discriminate between the different DNA bases (12–17). In this case, a lipid membrane separates two reservoirs, the *cis* and the *trans* chambers, and the nanopore is embedded in the membrane, providing the only passage for DNA and ions from the *cis* to the *trans* side. Ionic current measurements are taken to monitor the passage of the biomolecule. The variation in the ionic current trace is then deciphered to reveal the sequence of the DNA. It has been demonstrated that solid-state nanopores have the ability to resolve differences in ionic current for short strands of different homopolymers (18), but they are still lagging in differentiating single bases.

One persisting issue when using nanopores for sequencing is the very high speed of the translocating biomolecule, which is typically of the order of $\sim$1 base/μs, as measured in experiments. This is too high for reliable detection of different nucleotides. Several methods have been developed to slow down translocation: modifying the DNA molecule (19,20), immobilizing DNA (21,22), adding hairpins or double-stranded DNA to the end of the ssDNA (23–25), employing dumbbell structures (26–28), modifying the viscosity of the solvent (29,30), varying temperature (31–33), adding charge modifications to the nanopore (12,34–36), and controlling the speed by mechanical force (10). Aside from charge-modified nanopores, these techniques are usually very complex and can modify the analytes or the buffer solution, which affects the ionic current signal. For these reasons, we focus on nanopore charge modifications in this work.

Extensive experimental work has already been done on the charge mutations of the α-hemolysin (αHL) nanopore, where additional charges are introduced in the β-barrel of the nanopore (see Fig. 1) by site-directed mutagenesis (12,34). It was shown that the average translocation speed of a short ssDNA can be much longer, without the need to change buffer solution or add secondary structures on the DNA or the nanopore. Although several theoretical and computational studies have been done about the interactions of polymers with attractive charged groups within ion channels and pores (37–40), there remain several unresolved

Submitted June 8, 2017, and accepted for publication August 21, 2017.
*Correspondence: muthu@polysci.umass.edu
Editor: Anatoly Kolomeisky.
http://dx.doi.org/10.1016/j.bpj.2017.08.045

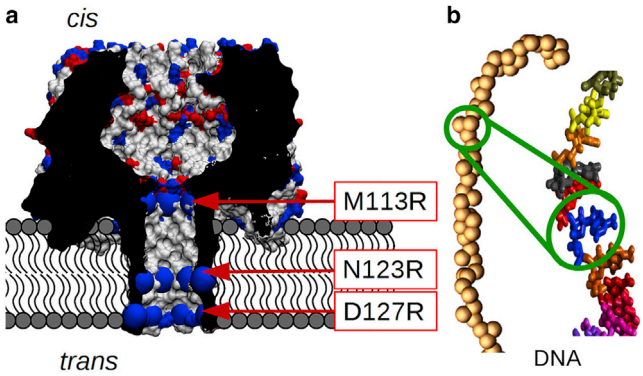

FIGURE 1 (*a*) The αHL protein pore, showing the location of mutations to add additional positive charges in the β-barrel region. The mutated amino acid residue is represented by blue beads that are positively charged. The red beads are negatively charged and the gray beads are neutral. (*b*) The ssDNA is modeled using three beads per nucleotide. To see this figure in color, go online.

concerns regarding the experimental results. First, it was unknown whether the bases translocate at a uniform speed. Additionally, the ionic current drops very low when there are too many charge mutations inside the β-barrel. This observation is still a puzzle. Tracking the movement of each base is not yet possible in experiments but can be easily achieved in simulations, bringing new insights into the dynamics of the DNA as it translocates.

In this work, we report extensive coarse-grained (CG) Langevin dynamics simulations of ssDNA translocating through wild-type and mutated αHL nanopores. To simulate DNA translocation, we modeled a protein nanopore, a membrane, an electrolyte solution, and an ssDNA. We calculated the trajectory of the DNA molecule using Langevin dynamics. We also constructed the electric potential profiles of each nanopore and incorporated it into our translocation simulations, which allows us to see how added charges modify the electric potential of the system and, hence, the energy of the system and the translocation dynamics of DNA.

This work is organized in the following manner. The next section details the methodology, with descriptions of the models and simulation setup. In Results and Discussion, the results are presented and discussed. A brief overview and summary of this work is given in the Conclusion.

METHODS

Models

We use the CG approach to model the ssDNA, the nanopore, and the membrane. This reduces the number of beads in the protein nanopore from ~20,330 to 2051, leading to at least a 100-fold decrease in calculation time. Consequently, we were able to carry out thousands of simulations to study the general behavior of translocation dynamics. Fig. 1 *a* shows the protein nanopore with the CG mutations used in this work and Fig. 1 *b* shows the ssDNA.

Instead of the single-bead approach, where each nucleotide is modeled as one bead, we modeled each nucleotide with three beads, following our previous work (41). Each nucleotide is made up of three beads, where one bead is for the phosphate group, one for the sugar, and one for the base, as shown in Fig. 1 *b*. The beads representing the sugar and the base are neutral. The bead representing the phosphate group has a charge $q = -1e$, where e is the elementary charge. Each bead has a diameter of 2.5 Å, so each nucleotide has a radius of 2.5 Å. The mass of the nucleotide is equally distributed to the three beads for simplicity, with each bead carrying 96 Da. The DNA we used has a total length of 45 nucleotides and is modeled as a homopolymer, since our present DNA model does not include any base-specific parameters.

The membrane that supports the protein nanopore is modeled as two layers of uncharged beads of radius 2.5 Å, each with a mass of 96 Da. The separation between the two layers is 50 Å, approximately the thickness of a lipid bilayer. Here, the membrane serves only as a separation between the *cis* and the *trans* sides of the nanopore. As such, the parameters of the membrane were chosen to coincide with that of the DNA for convenience.

The wild-type (WT) heptameric three-dimensional αHL structure used is Protein Data Bank entry PDB: 7AHL (42). The CG protein is obtained by representing all the atoms within the same amino acid residue as one single bead. The missing hydrogens and the size of each atom are inserted and determined using PDB: 2PQR (43,44). Thus, the radius of each residue bead is the distance from its center of mass to its farthest atom, plus the radius of that farthest atom. This residue bead has a radius that is large enough to encapsulate all the atoms belonging to that residue. The mass of each residue bead is the mass of the corresponding amino acid as reported in the literature (45). There are some residues that can be either positively or negatively charged due to their side chains and depending on the solution pH. The list of amino acid residues and their properties can be found in the literature (45). The net charge of the residue bead is determined through the negative of the logarithm of the acid dissociation constants for COOH, NH_2 groups, and the side chain (45). This net charge is also compared with theoretical calculations from PDB: 2PQR (43,44) to ensure consistency. In this work, we use residue charges at pH 8. More details on the CG method as applied to protein permeation can be found in an earlier work (46).

There are several mutant αHL pores studied in this work, following the pioneering experimental work of Maglia et al. (12): RL2, RL2-M113R, RL2-N123R, RL2-M113R-N123R, and RL2-N123R-D127R. The RL2 nanopore differs from the WT due to the mutations V124L, G130S, N139Q, I142L, and K8A. In these mutation notations, the first letter represents the original amino acid residue, the number that follows is its location on the polypeptide chain, and the last letter is the amino acid residue that replaced it. Note that there is no additional charge decoration in the β-barrel between WT and RL2. Further mutations on the RL2 pore replace the neutral residue with positively charged arginines. For example, RL2-M113R-N123R has two arginines mutated at amino acid residues 113 and 123 on each monomer of the heptameric protein. We perform the residue mutations on the CG protein. For the M113R and N123R mutations, a total charge of $+14e$ is added to the β-barrel, since each arginine has a $+1e$ charge and a total of 14 arginines are added into the barrel. These mutations modify the charge pattern along the β-barrel to slow down the translocation dynamics of DNA.

Simulation details

We use the Langevin dynamics approach to track the movement of the DNA as it moves through the system. This approach replaces the explicit force from each water molecule with a stochastic force that represents the net force due to the water molecules at a given time. The nanopore and the membrane are treated as a rigid body fixed in space, so interactions among beads of the nanopore and the membrane are not considered. Langevin dynamics of DNA undergoing translocation through the protein nanopore in the presence of an external electric field is performed using the LAMMPS (47) package. The trajectory of the DNA is calculated by integrating the Langevin dynamics of the ith bead of the DNA:

$$m\frac{d^2\vec{r}_i}{dt^2} = -\zeta\frac{d\vec{r}_i}{dt} - \nabla_i U(\vec{r}_i) + \vec{F}_i(t), \quad (1)$$

where m is the mass of each DNA bead, $\vec{r}_i$ is the position of the ith bead, ζ is the friction coefficient, U is the total potential energy acting on the ith bead, and $\vec{F}_i(t)$ is the stochastic force acting on the bead. The random force term, $\vec{F}_i(t)$, is the net force due to the solvent molecules acting on the ith bead at time t, satisfying the fluctuation-dissipation theorem:

$$\left\langle \vec{F}_i(t) \cdot \vec{F}_j(t') \right\rangle = 6k_B T\zeta\delta_{ij}\delta(t-t'), \quad (2)$$

where k_B is the Boltzmann constant, $T = 298$ K is the temperature, and $\delta(t)$ is the Dirac delta function. The value of the friction coefficient sets the timescale for the dynamics. In Eq. 1, the coefficient was fixed arbitrarily as 1 in the simulation reduced unit for simplicity, since we do not know the drag coefficient for each bead of the nucleotide. As a result, the timescale is arbitrary in the Langevin dynamics simulations. This is why we need to set the timescale by comparing with experiments. However, we made sure that the fluctuation-dissipation theorem is satisfied.

The total potential energy, U, acting on the ith bead can be written as follows:

$$U = U_S + U_B + U_{LJ} + U_C + q\Phi, \quad (3)$$

where U_S, U_B, U_{LJ}, U_C, and $q\Phi$ are the different interaction potentials present in the system.

The spring bonding potential, $U_S = k_s(r_s - r_0)^2$ acts between connected beads, where $k_s = 171$ kcal/mol$\cdot$Å^2 is the spring constant (41), r_s is the distance between the ith bead and its adjacent bead, and $r_0 = 2.5$ Å is the equilibrium distance. The bending angle potential, $U_B = k_a[\cos(\theta) - \cos(\theta_0)]^2$, is between the side chain and the backbone, where $k_a = 60$ kcal/mol is the bond angle constant (48), θ is the angle between the side chain and the phosphate backbone, and $\theta_0 = 65^\circ$ is the equilibrium bond angle (48). The Lennard Jones (LJ) potential, $U_{LJ} = 4\epsilon[(\sigma/r)^{12} - (\sigma/r)^6] + \epsilon$, models the excluded-volume interactions, where $\epsilon = 0.5$ kcal/mol, $\sigma = 2.5$ Å, and r is the distance between the ith bead and the jth bead of the system. The LJ potential is truncated at $r = r_c$, where $r_c = 1.12\sigma$. For the LJ interactions between DNA and the membrane bead or the nanopore bead, the σ values used are summarized in Table S2. The screened Coulomb potential, $U_C = (qq_j/4\pi\varepsilon r)\exp(-\kappa r)$, is modeled using the Debye-Hückel potential, where q_j is the charge of the jth bead in the system, $\kappa = L_D^{-1} = 0.325$ Å^{-1} is the inverse Debye length of 1 M KCl, $\varepsilon = \varepsilon_0\varepsilon_r$ is the permittivity, $\varepsilon_r = 2$ in the protein and the lipid bilayer and 80 everywhere else, and ε_0 is the permittivity of free space. As the main focus of this work is to understand the translocation dynamics of DNA through the β-barrel, the simulation starts with DNA partially inside the vestibule cavity to reduce unnecessary simulation time during the capture stage.

An external applied potential difference of 120 mV is applied between the *cis* and *trans* chambers of the system. The electrostatic potential of the system as a result of the applied potential, charges in the nanopore, and ions in the solution is calculated using the Poisson-Nernst-Plank (PNP) formalism (49–52). The last term of Eq. 3 is the electrostatic potential of the system, where q is the charge of the ith bead and Φ is the electrostatic potential through the pore, computed using the PNP procedure, which couples the steady-state Poisson equation with the Nernst-Planck equations. This is done by solving self-consistently the Poisson equation,

$$\nabla \cdot [\varepsilon(\vec{r})\nabla\Phi(\vec{r})] = -\rho_p(\vec{r}) - \rho_e(\vec{r}), \quad (4)$$

together with the steady-state Nernst-Planck equation,

$$\nabla \cdot \left[\nabla C_n + \frac{Z_n C_n}{k_B T}\nabla\Phi(\vec{r})\right] = 0, \quad (5)$$

to obtain the local concentrations of the cations and anions following procedures similar to those discussed in the literature (41,53). In Eq. 4, $\varepsilon = 2$ in protein, DNA, and membrane and 80 everywhere else. In Eq. 5, $n = \{K^+, Cl^-\}$ are the ions in the solution, and $Z_n = 1e$ or $-1e$, depending on the ion species. The charge densities in Eq. 4 are due to all the fixed charges in the system, such as the charges on the protein, ρ_p, and the mobile ions in the solution, ρ_e, where $\rho_e(\vec{r}) = e[C_{K^+}(\vec{r}) - C_{Cl^-}(\vec{r})]$. The electrostatic potentials calculated using Eqs. 4 and 5 are shown in Fig. 2. The potential is along the center of the nanopore at $[0, 0, z]$ for the different nanopores considered.

The simulation is realized by first relaxing the DNA in the absence of external potential and protein pore. During the relaxation stage, Eq. 3 does not include the last term, $q\Phi$, and U_{LJ} and U_C are only interactions among the beads of the DNA. The nanopore is then inserted into the simulation box for the translocation process. At this stage, all terms of Eq. 3 are included in the simulation. There are at least 1000 simulations performed for each of the nanopores described in this work. By using a normal fit, we obtain the most likely translocation time as the maximum of the fit to the translocation time distribution, which coincides with the average of the distribution.

To assess the ionic current during a translocation simulation, the PNP is solved for each position of the DNA at each time step of the simulation. The coordinates of the DNA and the nanopore are entered as ρ_p into Eq. 4 to solve for the ion concentrations, C_n, and the potential, Φ. The ionic current is then given by

$$I(t) = \int d^2\vec{r}(J_+ + J_-), \quad (6)$$

where the ionic flux of the cations (J_+) or the anions (J_-) is determined by

$$J_\pm(\vec{r}, t) = -D_\pm\left[\nabla C_\pm + \frac{Z_\pm C_\pm}{k_B T}\nabla\Phi(\vec{r})\right], \quad (7)$$

where D is the diffusion coefficient of the respective ionic species: $D_+ = 1.96 \times 10^{-5}$ cm$^2\cdot$s^{-1} and $D_- = 2.03 \times 10^{-5}$ cm$^2\cdot$s^{-1} (45). The areas integrated over in Eq. 6 represent the circular cross-sectional area of different radii along the z axis of the nanopore, yielding slightly different

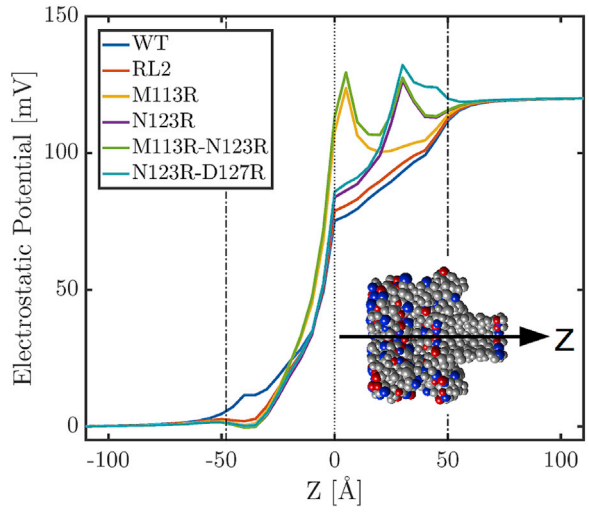

FIGURE 2 Electrostatic potentials along the center of the αHL pore from the *cis* to the *trans* side. The vestibule entrance at $z = -48$ Å and the β-barrel end at $z = 48$ Å are marked by dashed lines in the plot. The bulk concentration is 1M KCl and the applied potential difference is 120 mV. The nanopore shown is a CG WT showing the direction of the z axis along the center of the pore. To see this figure in color, go online.

values of I along the z axis. These values of I are then averaged over z to give $\bar{I}$ at time t.

RESULTS AND DISCUSSION

Electrostatic potentials

We start our investigation by examining the electrostatic potential through each nanopore, as shown in Fig. 2. The computed electric potential given in Fig. 2 is for the model presented here when the charges are localized on individual beads. In reality, the charges are smeared out and the peaks in the electric potential profile would analogously be rounded off. Naturally, there are no diverging electric fields in the system. The WT and RL2 pores do not have additional positive charges in the β-barrel and have similar, nearly monotonic electrostatic potential profiles. When positive charges are added to the barrel, the electrostatic potential is modified accordingly and shows peaks at the corresponding locations of the added charges. For one positive charge mutation, such as the M113R and N123R nanopores, one single peak appears at the corresponding location of the charge. For nanopores with two charge mutations, such as M113R-N123R and N123R-D127R, two peaks show up in the potential profiles. In the case of the M113R-N123R nanopore, the two charge mutations are 10 amino acid residues apart and the corresponding peaks are well separated. For the N123R-D127R nanopore, the two charge mutations are only four residues apart, so the peaks overlap. Note that in Eq. 4, the electrostatic potentials are calculated in the absence of the DNA. The goal of this work is to understand how charge decoration affects local dynamics during translocation of the DNA, with the ultimate goal of designing the optimal charge patterning for DNA sequencing.

Comparison with experiments

First, we calculate the translocation time per nucleotide through each nanopore (t_n). This is shown in Fig. 3. Each distribution is fit with a Gaussian form (Fig. 3, *inset*), from which the peak determines the most likely translocation time. For both WT and RL2 pores, the distribution of t_n is highly localized, there is little variation, and both nanopores have the same most likely translocation time. This confirms that the translocation time is not affected by uncharged residue mutations, but rather is highly dependent on the electrostatic interaction between DNA and the nanopore. For nanopores with one charge mutation, the most likely translocation time becomes larger and the distribution becomes wider, with the peaks of both distributions coinciding. This shows that the addition of one charge mutation can increase t_n, regardless of the mutation location along the β-barrel. For nanopores with two charge mutations, the t_n distributions are much more spread out and the average translocation time is much larger.

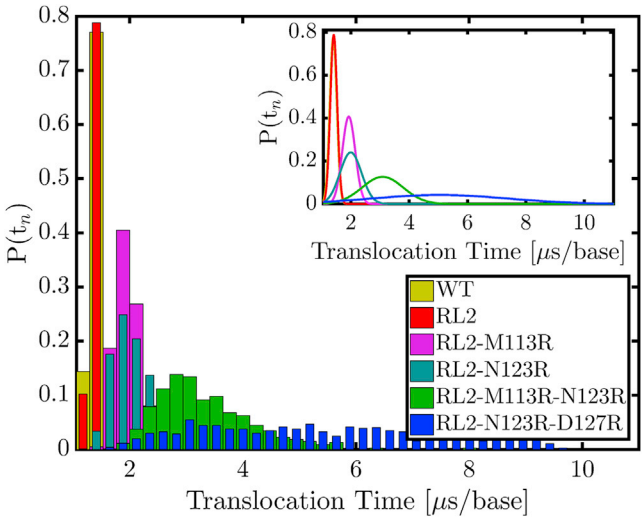

FIGURE 3 Distribution of the translocation time per nucleotide of the DNA. This is the time taken for the entire chain of DNA to exit the β-barrel divided by the number of nucleotides. The most likely translocation time is taken as the maximum of the Gaussian fit shown in the insets and in Table S1. To see this figure in color, go online.

We compared our simulation results to the experimental values (34), which are summarized in Table S1 and in Fig. 4. Since in our Langevin dynamics simulations the time unit is arbitrary, we can set this time by calibrating the simulation value with the experimental values for the WT and RL2 nanopores. After setting the timescale with this one parameter, namely by multiplying our simulation time by a factor of 0.106 μs, no more adjustment of the timescale is needed. As seen in Table S1, our results agree well with the experimental values. This verifies that our CG approach captures the relevant behavior of the biomolecule.

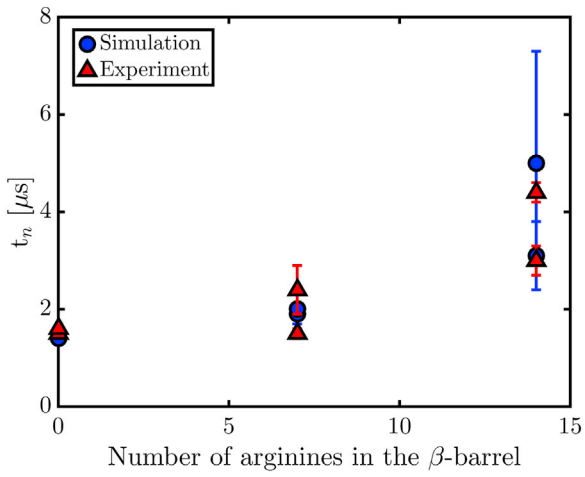

FIGURE 4 Comparison between simulation and experimental results (34) of the most likely translocation time per nucleotide (t_n) for different charge decorations of the nanopore. The simulated system was performed for 1M KCl at 300 K with an external potential difference of +120 mV. To see this figure in color, go online.

Ionic current traces

Next, we examine the ionic current trace of a typical trajectory of DNA translocating through the RL2 nanopore and through a decorated nanopore, RL2-M113R-N123R, as shown in Figs. 5 and 6, respectively. From our calculations, we see that the open-pore current of RL2 is ~110 pA, which is slightly higher than the ~90 pA of the mutated pore. The trace in Fig. 5 and the simulation snapshots show the stages of the translocation process through an RL2 nanopore. First, the DNA fills up the vestibule (Fig. 5, *S1*) and spends some time in the vestibule, as it needs to cross the entropic barrier to enter the barrel (54). During this stage, the DNA can sometimes return to the *cis* side, leaving the nanopore completely. The ionic current is affected as soon as the DNA is near the pore and blocking the entrance to the vestibule, not necessarily inside the vestibule yet. In the second stage (Fig. 5, *S2*), DNA finds the barrel entrance, crosses the entropic barrier, and enters the β-barrel. At this point, the translocation process is most likely to be completed with very low probability of the DNA reversing direction back to the vestibule. Although DNA is inside the barrel, the ionic current drops significantly, to an average around 16 pA. In experiments, as DNA is moving through the barrel, the accessible cross-sectional area inside the barrel is greatly reduced due to the presence of the DNA, allowing a very low number of ions to pass, and the ionic current is very low. Soon after this, DNA starts emptying from the β-barrel to the *trans* chamber, where the majority of the DNA has already translocated to the *trans* side (Fig. 5, *S3*). Sometimes the DNA does not move far away from the barrel exit, and it can create a jamming effect at the exit, hindering the egress of the tail of the DNA chain. The ionic current starts rising as soon as the DNA is leaving the nanopore and can go back down when DNA lingers in the barrel. In the last stage, DNA translocates through the nanopore completely, and the current level is restored to the open-pore level (Fig. 5, *S4*). See also Movie S1, which shows DNA translocation through the RL2 nanopore.

For DNA translocating through a charge-decorated pore, the stages are similar to those described in the previous paragraph, with some modifications. The vestibule-filling stage (Fig. 6, *M1*) is comparable to that for the undecorated nanopore, and DNA enters the barrel in a similar fashion. The electric potential of the mutated pore rises higher inside the barrel, as shown in Fig. 2, indicating a stronger electric field and hence stronger force on the charged polymer inside the β-barrel. The electrostatic interactions are expected to be dominant when DNA is inside the barrel due to electrostatic screening. In the second stage (Fig. 6, *M2*), as DNA is translocating through the barrel, the ionic current drops to almost zero, with an average around 0.2 pA. This becomes especially low when DNA is occupying the entire barrel and part of the vestibule, as shown in Fig. 6 (*M3*). The presence of DNA reduces the effective volume inside the nanopore, in turn reducing the volume accessible to the ions. In addition, the mutations also reduce the available volume, since arginines are bulkier than the residues they replaced. Furthermore, from our simulations, we see that when DNA is in the vicinity of charge decorations, it coils more than usual, which also contributes to higher blockage of ions. As DNA leaves the vestibule (Fig. 6, *M3*) and enters completely into the barrel, the ionic current slowly rises to an average of ~20 pA as the rest of the DNA slowly translocates through to the end of the barrel. Interestingly, we observe that ~12 nucleotides remain much longer in the barrel (Fig. 6, *M3*). Note that ~10–15 can fit in the barrel (55). When DNA finally completes translocation, the ionic current goes back to the open-pore level. See also Movie S2, which shows DNA translocation through the RL2-M113R-N123R nanopore.

Dynamics along the DNA

From the ionic current analysis, we see that DNA does not translocate with a uniform speed and sometimes gets

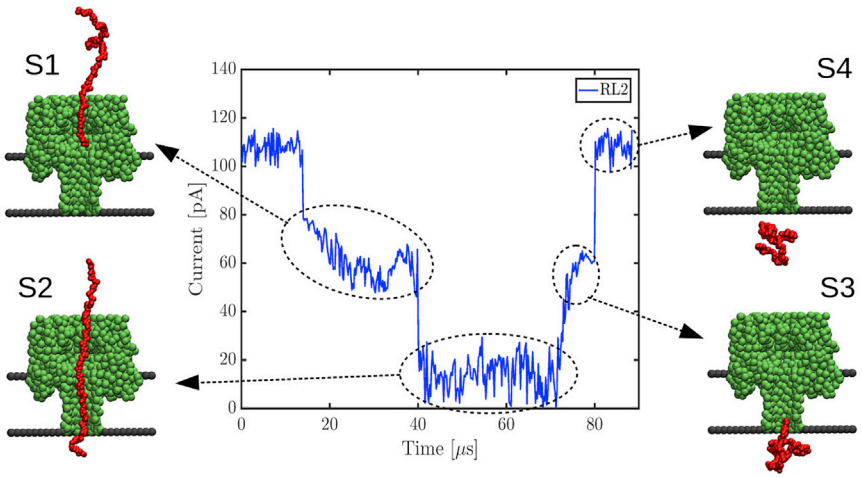

FIGURE 5 Ionic current trace through an RL2 nanopore as DNA translocates through the RL2 nanopore. The snapshots S1–S4 show the positions of the DNA during the various stages of translocation. To see this figure in color, go online.

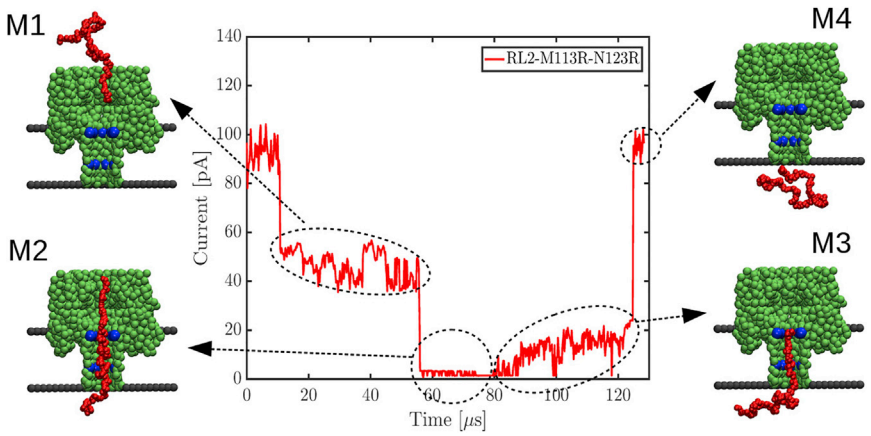

FIGURE 6 Ionic current trace as DNA translocates through an RL2-M113R-N123R nanopore. The blue spheres are the positively charged amino acid residues added by the mutations. The stages of DNA translocation are shown in snapshots M1–M4 at the corresponding current values. To see this figure in color, go online.

trapped for some time before exiting. To have a better understanding of how fast a portion of the DNA chain is translocating, we proceed to examine the translocation time per base of different segments along the DNA, as shown in Fig. 7. Segments a, b, and c, correspond to nucleotides 1–5, 31–35, and 41–45, respectively. These segments are chosen so that we can inspect the translocation dynamics at the beginning of translocation, before the DNA is trapped, and while DNA is trapped.

The distribution of translocation time per base of each segment (Fig. 8) reveals the dominant effect that electrostatic interactions have on translocation dynamics of DNA. For different nanopores, the translocation time distributions of segment a, as shown in Fig. 8 *a*, are all similar to each other. For the head of DNA, the electrostatic interactions do not have a significant effect on its dynamics. The entropic barrier of the barrel entrance and the unraveling dynamics are the dominant factors affecting translocation dynamics of the DNA.

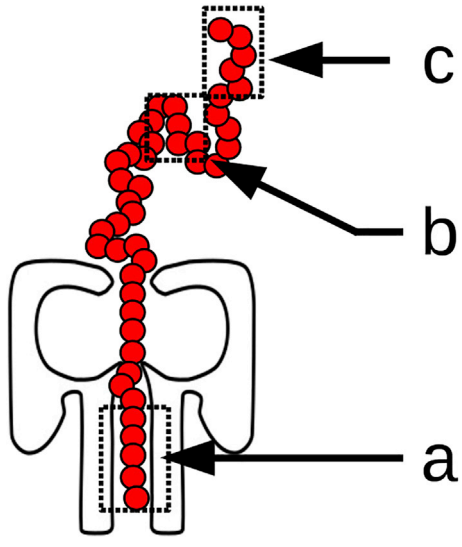

FIGURE 7 Segments a, b, and c of the DNA. Segments a–c correspond to nucleotide numbers 1–5, 31–35, and 41–45, respectively. To see this figure in color, go online.

For segment b of the DNA, the translocation times show a very different trend (see Fig. 8 *b*). Here, we see that for WT and RL2 nanopores, the translocation time of segment b is similar, as there are no additional charges in either barrel. For these two pores, segment b's translocation time is slightly shorter than that of the respective segments a; this is as expected, as there is almost no unraveling needed before the polymer translocates. The average translocation times of segment b through RL2-N123R and RL2-N123R-D127R are both less than those through RL2-M113R and RL2-M113R-N123R. For this portion of the DNA, the translocation time depends more on the location of the charge decoration and less on the number of charge decorations.

By the time segment c enters the barrel, a majority of the DNA has exited to the *trans* side. The average translocation time per base of segment c is shown in Fig. 8 *c*. For the WT and RL2 nanopores, the dynamics of segment c are similar to those of segment b, with the average translocation times comparable to those before. For nanopores with charge decorations, the translocation time of segment c becomes highly dependent on the number of charge decorations inside the barrel. The similarity in the time distributions of RL2-M113R and RL2-N123R shows that electrostatic interaction is the dominating factor affecting translocation. It also explains why the translocation times through RL2-M113R-N123R and RL2-N123R-D127R nanopores are longer than those through RL2-M113R and RL2-N123R. As for the RL2-N123R-D127R nanopore, the charge mutations are very close to each other, resulting in a much larger electrostatic potential barrier and much more difficulty for DNA to escape. The DNA is trapped for a much longer time, and its escape at this point becomes a random event, as demonstrated by the distribution.

Overall, we can make the following conclusions regarding the dynamics along the DNA. We do not see a much longer translocation time for segment a because there are many more beads after it that are also experiencing the

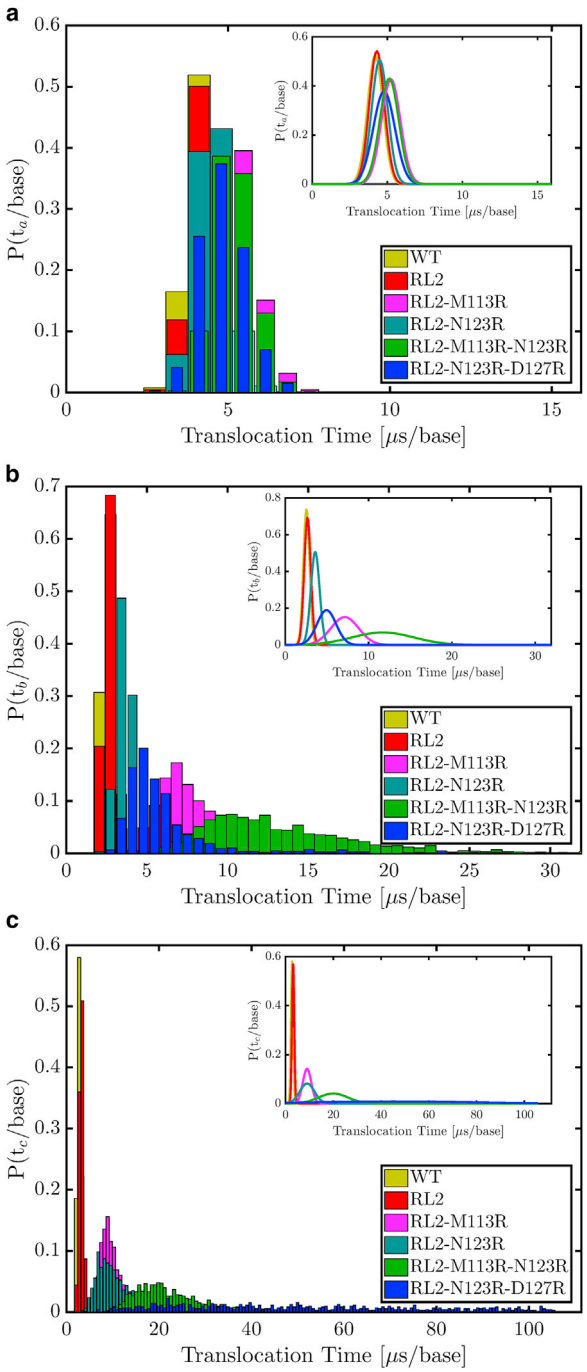

FIGURE 8 Distribution of the translocation times through the β-barrel per nucleotide for segments a (*a*), b (*b*), and c (*c*) of the DNA. The insets show the Gaussian fit to the corresponding distribution. To see this figure in color, go online.

electrostatic potential, moving forward and simply pushing segment a out of the way. We do see from Fig. 8 *a* that with charge decorations inside the barrel, the translocation times for segment a are slightly longer than those for WT and RL2 due to Coulomb interactions inside the barrel. However, for segments b and c, as they translocate through the barrel, there are many fewer beads, or almost no beads, to push them out of the way, allowing Coulomb interactions to dominate; hence, the translocation times vary with the number of charge mutations.

We can now consider the average translocation speed of each nucleotide of the DNA, as shown in Fig. 9, along with the standard deviations of two cases for comparison. This speed is obtained by calculating the time it takes for each nucleotide to travel through the 48 Å barrel, then averaging over all the simulations performed. We can see from Fig. 9 that DNA translocates through the nanopore with nonuniform speed. In general, DNA first accelerates then decelerates as it moves through the β-barrel. Through the WT and RL2 nanopores, the translocation speed of DNA increases as the number of untranslocated bases decreases. The speed then decreases when all the bases have either entered the barrel or successfully translocated to the *trans* chamber. For the undecorated nanopores, the free energy of the system is dominated by the entropic energy of the DNA chain, and the observed translocation dynamics have been studied extensively (48,56).

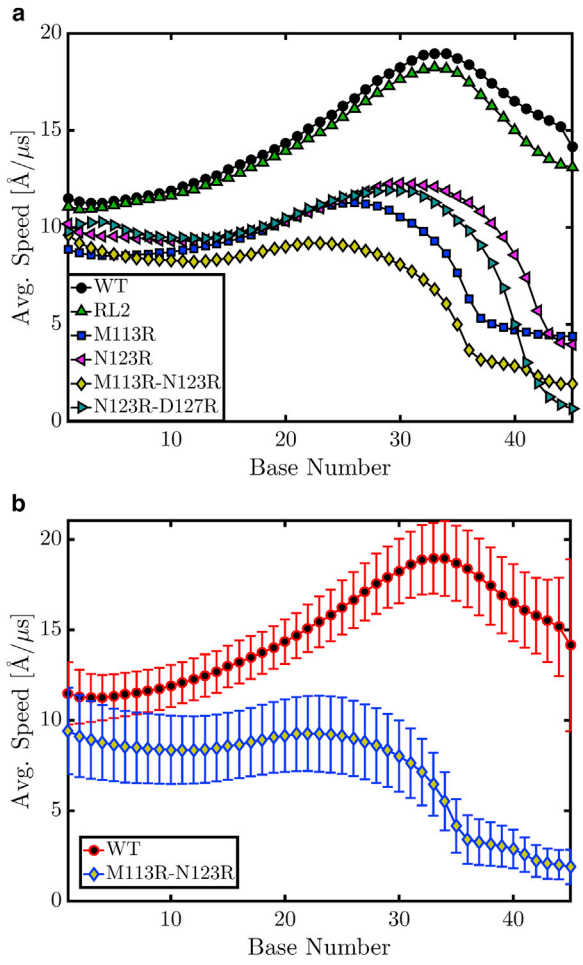

FIGURE 9 The average translocation speed of each nucleotide in the z-direction when inside the β-barrel are shown in *a*. The standard deviations of each nucleotide for the cases of WT and M113R-N123R are shown in *b*. To see this figure in color, go online.

For the decorated nanopore, the DNA translocation dynamics is predominantly affected by the charge interactions between the DNA and the mutated residues. In particular, the N123R nanopore can slow down translocation speed by >50%, but can only do so effectively at the tail of the DNA. The M113R nanopore can also slow down the speed of the DNA tail by >50% and has smaller variations in the traslocation speed. The N123R-D127R nanopore can slow translocation speed to close to zero, but it is only able to do so at the DNA tail. The only nanopore that steadily slows down DNA is M113R-N123R. As DNA translocates through this nanopore, it slows down gradually, then it traps the end of the DNA like the other decorated pore. A charge pattern similar to that observed for M113R-N123R could be a viable option for controlling DNA motion.

CONCLUSION

We have studied the translocation dynamics of DNA through various mutants of the αHL nanopore: RL2, RL2-M113R, RL2-N123R, RL2-M113R-N123R and RL2-N123R-D127R. The controls are the WT and RL2 nanopores, where the β-barrels are in the native state. For the nanopores with charge mutations, the modified electrostatic potential hinders the translocation of DNA. Our simulation results agree well with the experimental results, where the average translocation time per base is significantly delayed due to the Coulombic interactions with the mutated residues. We also observed the very low residual current while DNA is translocating through charge-decorated nanopores. Our simulations show that the low current is partly due to the coiling of the DNA while in close vicinity to the charge decorations, which reduces the volume accessible to ions. Another reason for the low residual current is the reduced volume accessible to ions due to the bulkier arginines introduced in the barrel. Most importantly, we observed that the bases do not translocate at a uniform speed. We demonstrated that the location of the charge mutations and distance between those mutations alters the velocity profile of the DNA. Our finding is a key consideration in designing optimal charge patterns in nanopores for DNA sequencing. Optimal charge patterns can also be designed in other types of nanopores for better control over DNA translocation, either by slowing down the DNA and/or by ensuring a constant translocation speed. Moreover, the translocation of charged polymers through nanopores is a ubiquitous process in biology (57–59), and the use of charge patterning could be applied in areas other than DNA sequencing.

SUPPORTING MATERIAL

One figure, three tables, and two movies are available at http://www.biophysj.org/biophysj/supplemental/S0006-3495(17)30968-2.

AUTHOR CONTRIBUTIONS

M.M. conceived and designed the project. I.J. carried out the simulations, data analysis and wrote the article with assistance from M.M.

ACKNOWLEDGMENTS

We are grateful for input from Kateryna Khairulina during the initial testing of the simulations.

This work was supported by grants from the National Science Foundation (DMR-1504265), National Institutes of Health (R01HG002776-12), and AFOSR (FA9550-14-1-0164).

REFERENCES

1. Gu, L. Q., and J. W. Shim. 2010. Single molecule sensing by nanopores and nanopore devices. *Analyst* (*Lond.*). 135:441–451.
2. Stoloff, D. H., and M. Wanunu. 2013. Recent trends in nanopores for biotechnology. *Curr. Opin. Biotechnol.* 24:699–704.
3. Feng, Y., Y. Zhang, …, C. Du. 2015. Nanopore-based fourth-generation DNA sequencing technology. *Genomics Proteomics Bioinformatics.* 13:4–16.
4. Arjmandi-Tash, H., L. A. Belyaeva, and G. F. Schneider. 2016. Single molecule detection with graphene and other two-dimensional materials: nanopores and beyond. *Chem. Soc. Rev.* 45:476–493.
5. Ivankin, A., R. Y. Henley, …, M. Wanunu. 2014. Label-free optical detection of biomolecular translocation through nanopore arrays. *ACS Nano.* 8:10774–10781.
6. Shim, J., G. I. Humphreys, …, R. Bashir. 2013. Detection and quantification of methylation in DNA using solid-state nanopores. *Sci. Rep.* 3:1389.
7. Buermans, H., and J. den Dunnen. 2014. Next generation sequencing technology: advances and applications. *Biochim.* Biophys. Acta. 1842:1932–1941.
8. Benner, S., R. J. A. Chen, …, M. Akeson. 2007. Sequence-specific detection of individual DNA polymerase complexes in real time using a nanopore. *Nat. Nanotechnol.* 2:718–724.
9. Kasianowicz, J. J., E. Brandin, …, D. W. Deamer. 1996. Characterization of individual polynucleotide molecules using a membrane channel. *Proc. Natl. Acad. Sci. USA.* 93:13770–13773.
10. Keyser, U. F. 2011. Controlling molecular transport through nanopores. *J. R. Soc. Interface.* 8:1369–1378.
11. Carson, S., and M. Wanunu. 2015. Challenges in DNA motion control and sequence readout using nanopore devices. *Nanotechnology.* 26:074004.
12. Maglia, G., M. R. Restrepo, …, H. Bayley. 2008. Enhanced translocation of single DNA molecules through α-hemolysin nanopores by manipulation of internal charge. *Proc. Natl. Acad. Sci. USA.* 105:19720–19725.
13. Stoddart, D., A. J. Heron, …, H. Bayley. 2010. Nucleobase recognition in ssDNA at the central constriction of the α-hemolysin pore. *Nano Lett.* 10:3633–3637.
14. Stoddart, D., G. Maglia, …, H. Bayley. 2010. Multiple base-recognition sites in a biological nanopore: two heads are better than one. *Angew. Chem. Int. Ed. Engl.* 49:556–559.
15. Butler, T. Z., M. Pavlenok, …, J. H. Gundlach. 2008. Single-molecule DNA detection with an engineered MspA protein nanopore. *Proc. Natl. Acad. Sci. USA.* 105:20647–20652.
16. Derrington, I. M., T. Z. Butler, …, J. H. Gundlach. 2010. Nanopore DNA sequencing with MspA. *Proc. Natl. Acad. Sci. USA.* 107:16060–16065.
17. Manrao, E. A., I. M. Derrington, …, J. H. Gundlach. 2011. Nucleotide discrimination with DNA immobilized in the MspA nanopore. *PLoS One.* 6:e25723.

18. Venta, K., G. Shemer, …, M. Drndić. 2013. Differentiation of short, single-stranded DNA homopolymers in solid-state nanopores. *ACS Nano.* 7:4629–4636.
19. Mitchell, N., and S. Howorka. 2008. Chemical tags facilitate the sensing of individual DNA strands with nanopores. *Angew. Chem. Int. Ed. Engl.* 47:5565–5568.
20. Henrickson, S. E., M. Misakian, …, J. J. Kasianowicz. 2000. Driven DNA transport into an asymmetric nanometer-scale pore. *Phys. Rev. Lett.* 85:3057–3060.
21. Purnell, R. F., K. K. Mehta, and J. J. Schmidt. 2008. Nucleotide identification and orientation discrimination of DNA homopolymers immobilized in a protein nanopore. *Nano Lett.* 8:3029–3034.
22. Purnell, R. F., and J. J. Schmidt. 2009. Discrimination of single base substitutions in a DNA strand immobilized in a biological nanopore. *ACS Nano.* 3:2533–2538.
23. Vercoutere, W., S. Winters-Hilt, …, M. Akeson. 2001. Rapid discrimination among individual DNA hairpin molecules at single-nucleotide resolution using an ion channel. *Nat. Biotechnol.* 19:248–252.
24. Vercoutere, W. A., S. Winters-Hilt, …, M. Akeson. 2003. Discrimination among individual Watson-Crick base pairs at the termini of single DNA hairpin molecules. *Nucleic Acids Res.* 31:1311–1318.
25. Lin, J., A. Kolomeisky, and A. Meller. 2010. Helix-coil kinetics of individual polyadenylic acid molecules in a protein channel. *Phys. Rev. Lett.* 104:158101.
26. Nakane, J., M. Wiggin, and A. Marziali. 2004. A nanosensor for transmembrane capture and identification of single nucleic acid molecules. *Biophys. J.* 87:615–621.
27. Tropini, C., and A. Marziali. 2007. Multi-nanopore force spectroscopy for DNA analysis. *Biophys. J.* 92:1632–1637.
28. Cockroft, S. L., J. Chu, …, M. R. Ghadiri. 2008. A single-molecule nanopore device detects DNA polymerase activity with single-nucleotide resolution. *J. Am. Chem. Soc.* 130:818–820.
29. Kawano, R., A. E. Schibel, …, H. S. White. 2009. Controlling the translocation of single-stranded DNA through α-hemolysin ion channels using viscosity. *Langmuir.* 25:1233–1237.
30. de Zoysa, R. S. S., D. A. Jayawardhana, …, X. Guan. 2009. Slowing DNA translocation through nanopores using a solution containing organic salts. *J. Phys. Chem. B.* 113:13332–13336.
31. Fologea, D., J. Uplinger, …, J. Li. 2005. Slowing DNA translocation in a solid-state nanopore. *Nano Lett.* 5:1734–1737.
32. Meller, A., and D. Branton. 2002. Single molecule measurements of DNA transport through a nanopore. *Electrophoresis.* 23:2583–2591.
33. Verschueren, D. V., M. P. Jonsson, and C. Dekker. 2015. Temperature dependence of DNA translocations through solid-state nanopores. *Nanotechnology.* 26:234004.
34. Rincon-Restrepo, M., E. Mikhailova, …, G. Maglia. 2011. Controlled translocation of individual DNA molecules through protein nanopores with engineered molecular brakes. *Nano Lett.* 11:746–750.
35. Bhattacharya, S., I. M. Derrington, …, A. Aksimentiev. 2012. Molecular dynamics study of MspA arginine mutants predicts slow DNA translocations and ion current blockades indicative of DNA sequence. *ACS Nano.* 6:6960–6968.
36. Katkar, H. H., and M. Muthukumar. 2014. Effect of charge patterns along a solid-state nanopore on polyelectrolyte translocation. *J. Chem. Phys.* 140:135102.
37. Kolomeisky, A. B. 2007. Channel-facilitated molecular transport across membranes: attraction, repulsion, and asymmetry. *Phys. Rev. Lett.* 98:048105.
38. Kolomeisky, A. B., and K. Uppulury. 2011. How interactions control molecular transport in channels. *J. Stat. Phys.* 142:1268–1276.
39. Berezhkovskii, A. M., M. A. Pustovoit, and S. M. Bezrukov. 2002. Channel-facilitated membrane transport: transit probability and interaction with the channel. *J. Chem. Phys.* 116:9952–9956.
40. Kasianowicz, J. J., T. L. Nguyen, and V. M. Stanford. 2006. Enhancing molecular flux through nanopores by means of attractive interactions. *Proc. Natl. Acad. Sci. USA.* 103:11431–11432.
41. Muthukumar, M., and C. Y. Kong. 2006. Simulation of polymer translocation through protein channels. *Proc. Natl. Acad. Sci. USA.* 103:5273–5278.
42. Song, L., M. R. Hobaugh, …, J. E. Gouaux. 1996. Structure of staphylococcal α-hemolysin, a heptameric transmembrane pore. *Science.* 274:1859–1866.
43. Dolinsky, T. J., J. E. Nielsen, …, N. A. Baker. 2004. PDB2PQR: an automated pipeline for the setup of Poisson-Boltzmann electrostatics calculations. *Nucleic Acids Res.* 32:W665–W667.
44. Dolinsky, T. J., P. Czodrowski, …, N. A. Baker. 2007. PDB2PQR: expanding and upgrading automated preparation of biomolecular structures for molecular simulations. *Nucleic Acids Res.* 35:W522–W525.
45. Haynes, W. M. 2016. CRC Handbook of Chemistry and Physics:. CRC Press, Boca Raton, Florida.
46. Jou, I. A., D. V. Melnikov, and M. E. Gracheva. 2016. Protein permeation through an electrically tunable membrane. *Nanotechnology.* 27:205201.
47. Plimpton, S. 1995. Fast parallel algorithms for short-range molecular dynamics. *J. Comput. Phys.* 117:1–19. http://lammps.sandia.gov.
48. Kong, C. Y., and M. Muthukumar. 2002. Modeling of polynucleotide translocation through protein pores and nanotubes. *Electrophoresis.* 23:2697–2703.
49. Im, W., and B. Roux. 2002. Ion permeation and selectivity of OmpF porin: a theoretical study based on molecular dynamics, Brownian dynamics, and continuum electrodiffusion theory. *J. Mol. Biol.* 322:851–869.
50. Eisenberg, R. S. 1996. Computing the field in proteins and channels. *J. Membr. Biol.* 150:1–25.
51. Corry, B., S. Kuyucak, and S. H. Chung. 2000. Tests of continuum theories as models of ion channels. II. Poisson-Nernst-Planck theory versus Brownian dynamics. *Biophys. J.* 78:2364–2381.
52. Kurnikova, M. G., R. D. Coalson, …, A. Nitzan. 1999. A lattice relaxation algorithm for three-dimensional Poisson-Nernst-Planck theory with application to ion transport through the gramicidin A channel. *Biophys. J.* 76:642–656.
53. Kong, C. Y., and M. Muthukumar. 2005. Simulations of stochastic sensing of proteins. *J. Am. Chem. Soc.* 127:18252–18261.
54. Muthukumar, M. 2007. Mechanism of DNA transport through pores. *Annu. Rev. Biophys. Biomol. Struct.* 36:435–450.
55. Deamer, D., M. Akeson, and D. Branton. 2016. Three decades of nanopore sequencing. *Nat. Biotechnol.* 34:518–524.
56. Kong, C. Y., and M. Muthukumar. 2004. Polymer translocation through a nanopore. II. Excluded volume effect. *J. Chem. Phys.* 120:3460–3466.
57. Mohammad, M. M., and L. Movileanu. 2008. Excursion of a single polypeptide into a protein pore: simple physics, but complicated biology. *Eur. Biophys. J.* 37:913–925.
58. Mohammad, M. M., S. Prakash, …, L. Movileanu. 2008. Controlling a single protein in a nanopore through electrostatic traps. *J. Am. Chem. Soc.* 130:4081–4088.
59. Bikwemu, R., A. J. Wolfe, …, L. Movileanu. 2010. Facilitated translocation of polypeptides through a single nanopore. *J. Phys. Condens. Matter.* 22:454117.